

Inter-relation Between TiO_2 Nanoparticles Size and Kind/Size of Dyes on the Mechanism and Conversion Efficiency of Dye Sensitized Solar Cells

BET results:

BET results are summarized in Table S1, which clearly indicate that there is a decrease in surface area that can be translated to the TiO_2 nanoparticle growth. Also, the autoclaving temperature has an impact on the pore size distribution of the TiO_2 film (see Figure S1). Increasing of these pore size let effective penetration of the electrolyte in TiO_2 film, but reduce the TiO_2 film surface area. In spite of the fact that A-210 pore size is appropriate for the N3 dye in solar cells, this size is not appropriate for larger T2 dye (0.5 nm larger than N3).

Table S1. Surface area, average particle size and porosity of samples autoclaved at different temperatures

TiO_2	Average particle size (nm)	Surface area ($m^2 g^{-1}$)	Langmuir surface area ($m^2 g^{-1}$)	t-Plot external surface area (m^2/g)	t-Plot micropore volume ($cm^3 g^{-1}$)	BJH Adsorption average pore width (nm)
A-210	49.0785	122.2532	167.5115	101.1070	0.009194	16.2346
C-250	96.2166	62.3593	90.4466	72.7572	0.007049	240.026

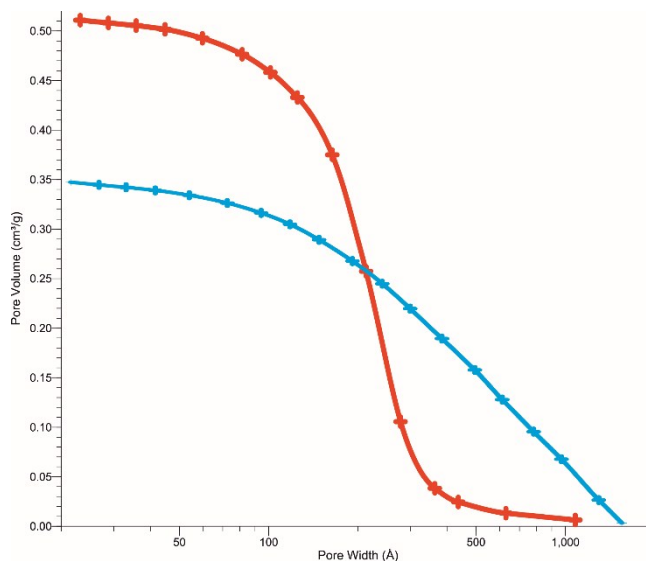


Figure S1. Cumulative pore size distributions of synthesized TiO_2 at 210°C (red line) and 250°C (blue line)

UV-visible absorption spectroscopy:

The UV-visible absorption spectra of TiO_2 films are shown in Figure S2a. The growth of TiO_2 nanoparticles size makes a red shift at the absorption edge of TiO_2 , which can be explained by the fact that an increase in the

particles size can cause a reduction in their band gaps.^{1, 2} The dyes adsorption on surface of the TiO_2 make another red shift at TiO_2 absorption edges and a blue shift (at their λ_{max}) for both N3 and T2 dyes (Figure S2b and c).

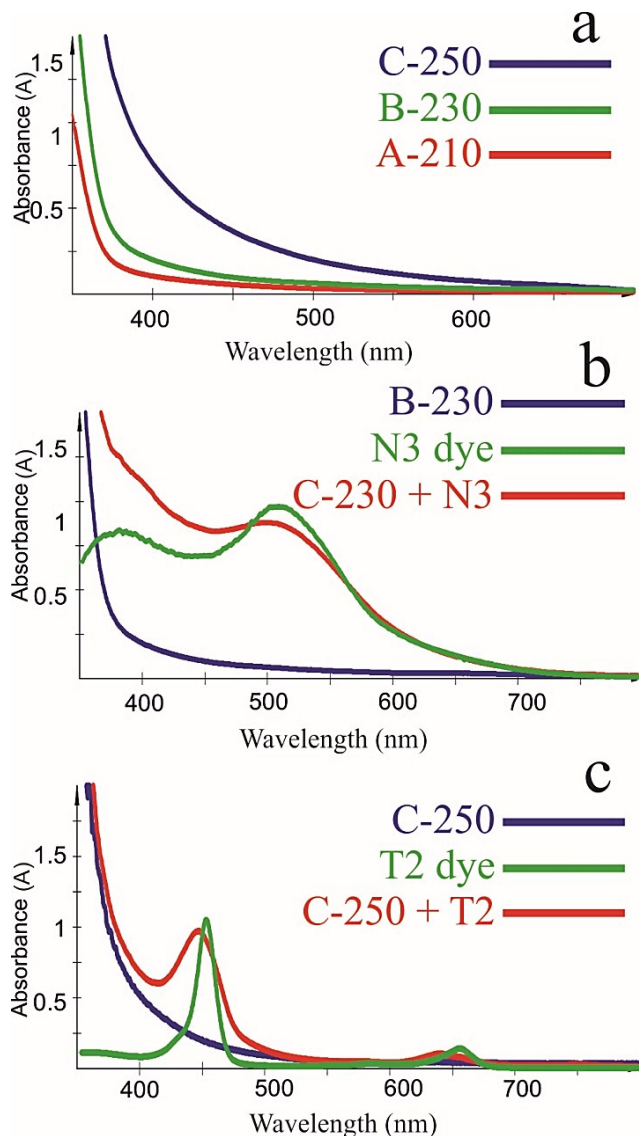


Figure S2. UV-visible absorption spectra of the TiO_2 films (a). UV-visible absorption spectra of the B-230 film, N3 dye in an ethanol solution and the film after N3 dye adsorption (b). UV-visible absorption spectra of C-250 film, T2 dye in a THF solution and the film after T2 dye adsorption(c).

Those red shift can be described by two different effects: first an electrostatic effect, which is caused by both, the protonation on the surface of TiO_2 and the dipole moment of the dye adsorbed on the TiO_2 surface, second a charge transfer effect between the dye and the TiO_2 surface.³ These electric fields and charge transfer effects facilitated the electron injections from the sensitizer to the TiO_2 conduction band, which can cause an increase in the current density of the DSSCs. However, these electric fields and charge transfers reduces the conduction-band potential, which lessening the open-circuit voltage at the DSSCs.⁴ The relationship between the conduction band potential (E_{CB}) and the quasi-Fermi level (E_{Fn}), which assigns the open-circuit voltage, are shown in Equation (5):⁵

$$E_{Fn} = E_{CB} + k_B T \ln \frac{n_c}{N_c} \quad (1S)$$

Where n_c is the charge density accumulated in TiO_2 and N_c is the effective density of states. Consequently, open-circuit voltage indirectly depends on the interaction between TiO_2 nanoparticles and dyes. On other hand, the deprotonation of dyes makes a blue shift at their λ_{max} , which has been investigated by Nazeeruddin et al. for ruthenium dyes.⁴

Dye aggregation:

UV-vis spectra of the aggregated T2 dyes are shown in Figure S3. The spectra of the aggregated dyes reveal that the sort and Q bands redshifted comparing with dyes in solution (6 nm and 9 nm respectively). On other hand, the adsorbed dyes on surface of the TiO_2 displayed blue-shifts in the UV-vis spectra (see Figure S2c). These results demonstrated that the dyes are not aggregated on surface of the TiO_2 photo-anode.

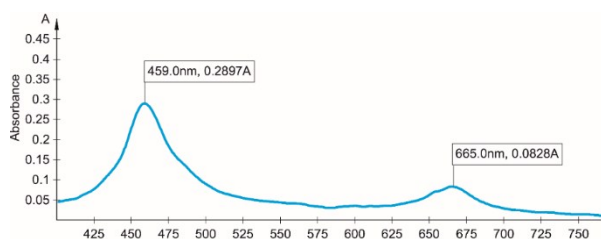


Figure S3. UV-vis spectra of the aggregated T2 dyes (sort = 459 and Q = 665 nm)

TiO_2 conduction band:

Figure S4. shows the CVs for the TiO_2 nanoparticles films after dividing the results current to the scan rate and subtraction the $R_s I_c$ terms from the operating potentials. The results reveal that the TiO_2 nanoparticles growth positively shifts the conduction band of TiO_2 films. This shift produces an increase of driving force for electron injection, though this gain is usually accompanied by an increase of photocurrent due to better efficient injection of photoexcited electrons.⁶ These results can be confirmed by the UV-vis absorption data, which are indicated TiO_2 absorption edges shifted toward higher wavelength. As previously reported,¹ these red shifts can be attributed to the reduce and increase of conductive and valance band of TiO_2 , respectively.

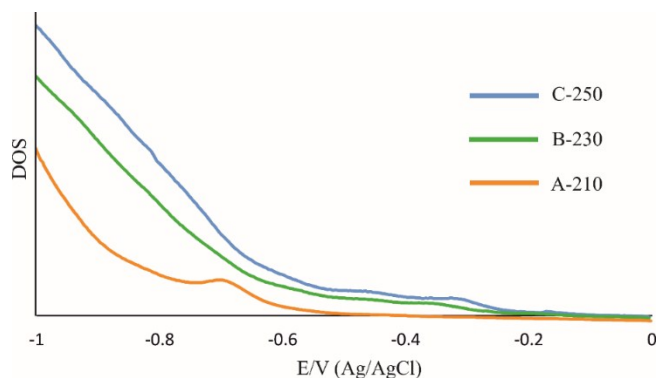


Figure S4. Conductive band of TiO_2 nanoparticles films calculated from CVs results

T1 dye Cells:

T1 dye⁷ is another porphyrin dye which its diameter is 0.2 nm lower than T2 dye (Figure S5). The fabricated cells with T1 showed similar results comparing with the T2 cells, where larger particle sizes enhance photovoltage and photocurrent (Figure S5). The J-V measurements of T1 dye were presented giving confidence that the pores diameter of TiO_2 photo-anode are not dominating factor for conversion efficiency of investigated porphyrin DSSCs.

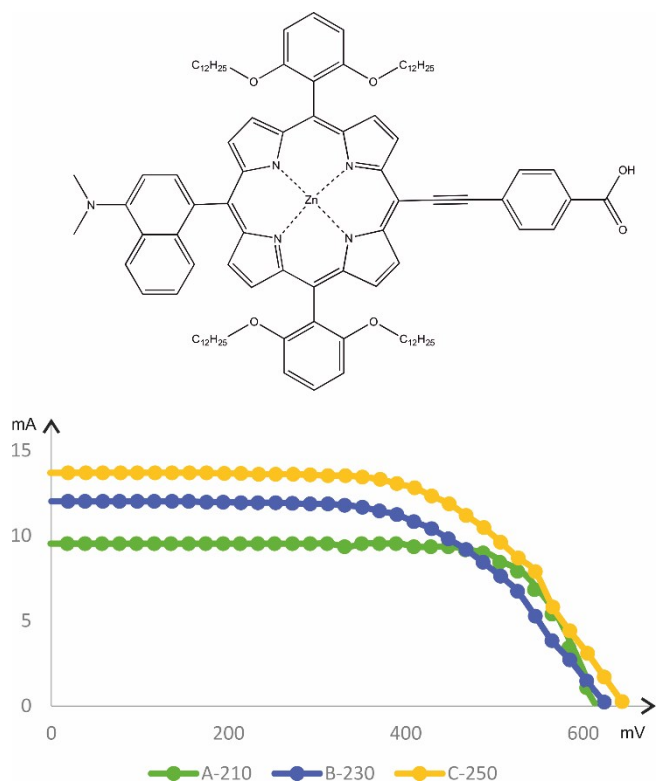


Figure S5. T1 dye molecular structure (top) J-V measurements of T1 DSSCs (bottom)

Impedance spectroscopy:

The obtained diagrams of impedance spectroscopy were fitted with EC-Lab software in terms of the equivalent circuit in Figure S6. The equivalent circuit is composed of parameters as follows: total series resistance of the substrate and solution (R_s), constant phase element of photo-electrode (CPE (1)), charge transfer resistance (R_{ch}), constant phase element of counter electrode (CPE (2)), charge transfer resistance of counter electrode (R_2) and diffusion impedance of $I^{-3/2}$ (Wd).

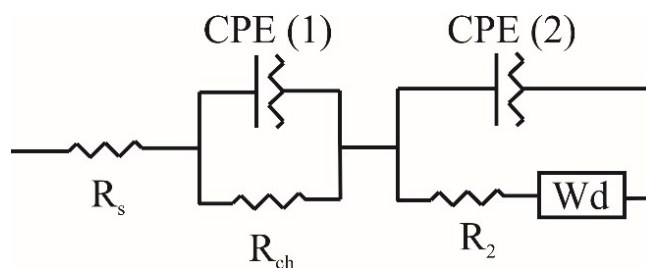


Figure S6. Equivalent circuit

Table S2. impedance fitting data of T2 solar cells. CPE and α mean the CPE constant and exponent, respectively. Rd and Td mean the resistance and time-constant of finite diffusion impedance.

TiO_2	R_s (Ω)	CPE (1) ($F.s^{(\alpha-1)}$)	α (1)	$R_{ch}(\Omega)$	CPE (2) ($F.s^{(\alpha-1)}$)	α (2)	R_2 (Ω)	Rd1 (Ω)	Td1 (s)
A-210	16.5	1.8×10^{-3}	0.9	15.1	4.1×10^{-5}	0.84	10.2	6.6	1.6
B-230	15.8	2×10^{-3}	0.87	8.6	3.6×10^{-5}	0.85	10.1	6	1.7
C-250	15.4	7×10^{-4}	0.85	10.3	3.2×10^{-5}	0.88	8.6	7.5	1.4

DFT calculation:

The Gaussian 09 package⁸ has been used to perform geometry optimization of T2 dye and the optimized geometry are used for perform timedependent calculation with B3LYP/6-31G(d). Figure S7 illustrates the electron density distributions of the dye in their respective HOMO, LUMO and triplet levels. Calculation results indicate that the triplet states energy of T2 dye in acetonitrile are close to TiO_2 conductive band.

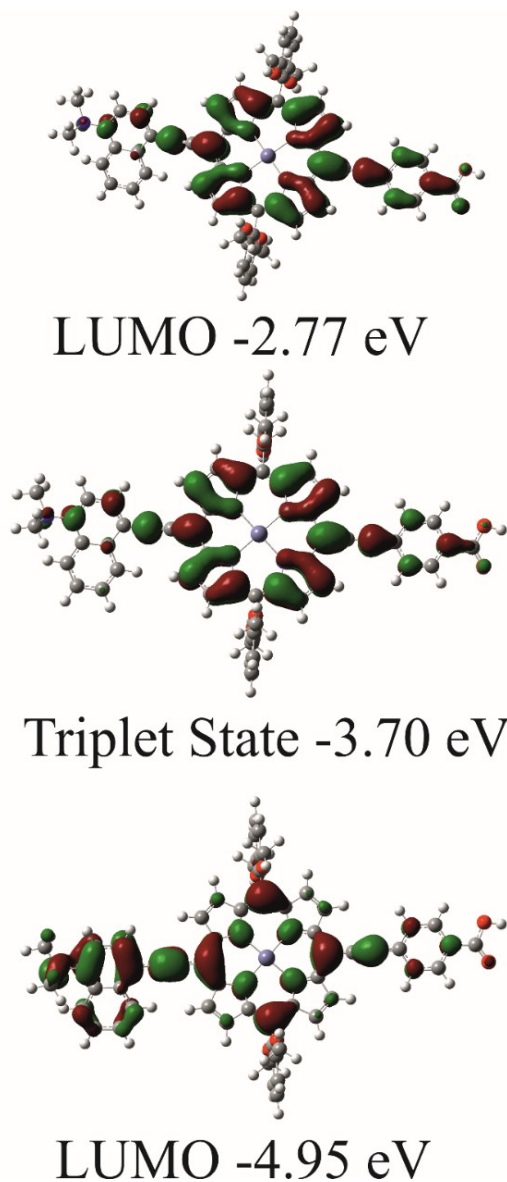


Figure S7. T2 dye electron density distributions in their respective HOMO, LUMO and triplet levels

References

1. H. Lin, C. P. Huang, W. Li, C. Ni, S. Ismat Shah and Y. Tseng, *Applied Catalysis B-Environmental*, 2006, **68**, 11.
2. N. Marom, T. Korzdorfer, X. G. Ren, A. Tkatchenko and J. R. Chelikowsky, *Journal of Physical Chemistry Letters*, 2014, **5**, 2395-2401.
3. E. Ronca, M. Pastore, L. Belpassi, F. Tarantelli and F. De Angelis, *Energy & Environmental Science*, 2013, **6**, 183-193.
4. M. K. Nazeeruddin, S. M. Zakeeruddin, R. Humphry-Baker, M. Jirousek, P. Liska, N. Vlachopoulos, V. Shklover, C. H. Fischer and M. Gratzel, *Inorganic Chemistry*, 1999, **38**, 6298-6305.
5. F. Fabregat-Santiago, G. Garcia-Belmonte, I. Mora-Sero and J. Bisquert, *Physical Chemistry Chemical Physics*, 2011, **13**, 9083-9118.

6. J. Bisquert, F. Fabregat-Santiago, I. Mora-Sero, G. Garcia-Belmonte, E. M. Barea and E. Palomares, *Inorganica Chimica Acta*, 2008, **361**, 684-698.
7. M. Adineh, P. Tahay, W.-K. Huang, H.-P. Wu, E. W.-G. Diau and N. Safari, *RSC Advances*, 2016, **6**, 102979-102983.
8. M. Frisch, G. Trucks, H. Schlegel, G. Scuseria, M. Robb, J. Cheeseman, G. Scalmani, V. Barone, B. Mennucci and G. Petersson, *Journal*, 2009.